Polymer Chemistry

Reversible Addition–Fragmentation Chain Transfer Step-Growth Polymerization with Commercially Available Inexpensive Bis-Maleimides

COMMUNICATION

Reversible Addition-Fragmentation Chain Transfer Step-Growth Polymerization with Commercially Available Inexpensive Bis-Maleimides

Parker T. Boeck,[a]† Noel E. Archer,[a] Joji Tanaka,*[a] and Wei You*[a].

Commercially available *N*-aromatic substituted bismaleimides were used in RAFT step-growth polymerization with a bifunctional RAFT agent, affording polymers having moderate to high molecular weights. This advancement increases the accessibility of our previously reported methodology and allows preparation of graft copolymers in a straightforward manner at significantly larger scale.
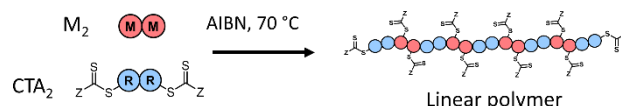
Step-growth polymerization offers great versatility in the design of the polymer backbone, a crucial feature that enables applications in drug delivery,[1] chemical recycling,[2] and solar cells.[3] However, traditional methods for step-growth typically require rather extreme reaction conditions and offer limited control over polymer architecture.[4] On the other hand, Reversible Addition-Fragmentation Chain-Transfer (RAFT) polymerization[5] has been widely adopted due to its adaptability and user-friendly nature to design polymers with controlled architecture;[6] however, the scope of the polymer backbone is typically limited to inert C-C single bond from vinyl monomers. To overcome these limitations, we have recently reported a RAFT step-growth polymerization,[7] which combines user-friendly nature of RAFT polymerization and versatility of polymer backbone.

The RAFT process is mediated by thiocarbonyl thioester-based Chain Transfer Agents (CTA) (that are also commonly called RAFT agents); CTA bears a fragmentable R group that generates radical (R•) adding to the monomer and Z-group that effects the radical reactivity of C=S bond. In a typical $A_2 + B_2$ type RAFT step-growth polymerization, bifunctional CTA and monomers are used under stoichiometrically balanced

conditions (**Scheme 1A**). The growth of polymeric chains is mediated by addition of the monomer functionality with fragmented CTA derived radical species (R•). The polymer backbone that is formed as a radical intermediate then proceeds to chain transfer with unreacted CTA functional group to regenerate R• species and form the polymer backbone (**Scheme S1**). This cyclic process is initiated through thermal

Scheme 1: RAFT step-growth polymerization in this work

A $A_2 + B_2$ RAFT Step growth polymerization

B Structure of **CTA₂**
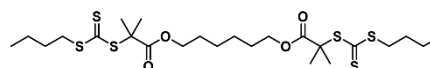
C Structure of M₂ in previous work

✗ **Multiple synthetic steps**
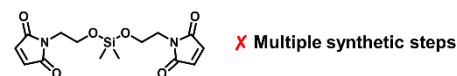
D Structure of M₂ in this work

M₂A
0.59 $/g

M₂B
0.82 $/g

M₂C
0.90 $/g

M₂D
0.55 $/g
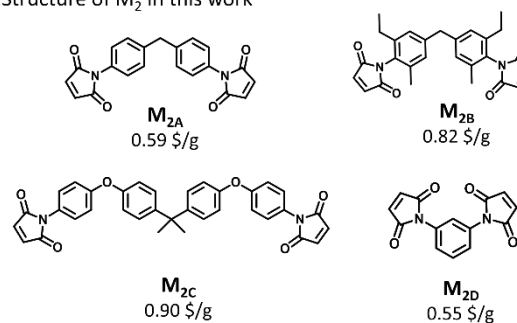
✓ **Commercially available and affordable**

[a.] *Department of Chemistry, University of North Carolina at Chapel Hill, Chapel Hill, NC, 27599-3290 USA*
† Current affiliation: Center for Catalysis, Department of Chemistry and George & Josephine Butler Polymer Research Laboratory, Center for Macromolecular Science & Engineering, Department of Chemistry, University of Florida, Gainesville, Florida 32611, United States

Figure 1. $A_2 + B_2$ RAFT step growth polymerization with **M2A** (A), **M2B** (B), **M2C** (C) and **M2D** (D) under stoichiometrically balanced conditions. The experimental weight averages (M_w, M_n, M_z) was determined by conventional SEC analysis in THF relative 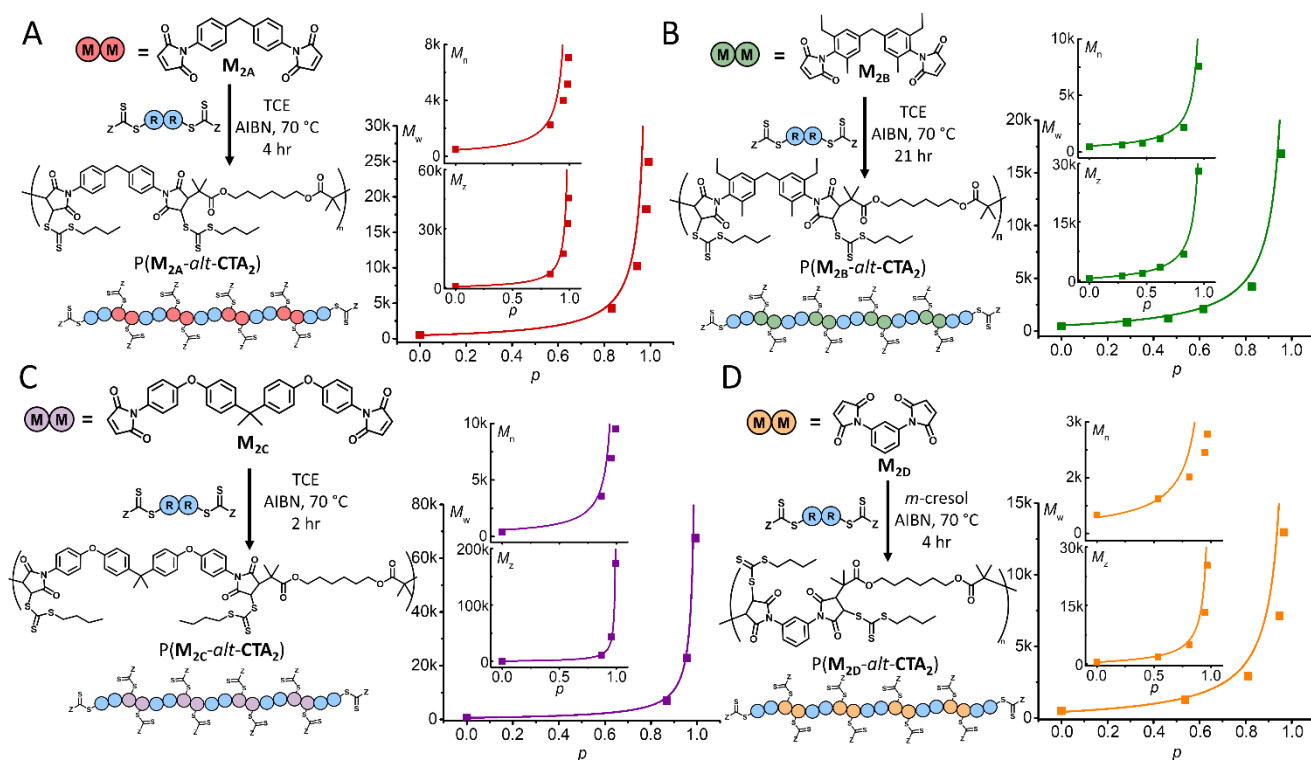to polystyrene standards. The extent of the reaction (p) is defined as monomer conversion of the maleimide determined by ^{1}H-NMR. Theoretical line was plotted with Eq. 1-3 without considering cyclization and initiator derived stochiometric imbalance.

decomposition of AIBN, forming the initial monomer-centered radical species (**Scheme S2**).

The step-growth evolution is achieved by rapid chain transfer of the CTA that bears a more radically stabilized fragmentable group (R•) than monomer centered radical species to drive the equilibrium and to prevent homopropagation of the monomer.[8] This requires suitable pairing of CTA and monomer reactivity that yields selective single monomer insertion under stoichiometrically balanced conditions. In the preceding literature, Moad,[9-11] Zard[12] and Xu[13-17] have exploited various pairing of monomers and CTAs for selective insertion process of a single monomer to CTA. In our initial report,[7] we found trithiocarbonate-based CTA bearing carbonyl ester stabilized tertiary radical fragmentable R-group and N-alkyl maleimidic monomer functionality to successfully allow RAFT step-growth polymerization.[7] It is noteworthy, in addition to our initial report, Zhu et. al. has recently demonstrated successful RAFT step-growth using xanthate-based CTA bearing carbonyl ester stabilized secondary radical fragmentable R-group and vinyl ether.[18]

The main draw-back of our original approach was the difficulty in preparing maleimidic monomer, which requires multiple synthetic steps (**Scheme 1C**). Fortunately, we found a series of commercially available and affordable N-aromatic bismaleimides (**Scheme 1D**). We envisioned the use of these monomers could expand the utility and scalability of our methodology. Herein, these bismaleimides were used directly without further purifications for $A_2 + B_2$ RAFT step-growth

polymerization with previously employed bifunctional CTA (**Scheme 1B**, **CTA2**).

We first examined the RAFT step-growth polymerization with N,N'-(1,4-Phenylene)dimaleimide, **M2A** as one of the most affordable monomers ($0.59/g from Tokyo Chemical Industry, TCI) in this study (**Figure 1A**). We employed tetrachloroethane (TCE) as the solvent rather than the previously employed dioxane, as most of the N-aromatic bismaleimides monomers investigated here have suitable solubility at the desired concentration in TCE. Following our stoichiometrically balanced reaction conditions in our initial work ([**CTA2**]$_0$: [**M2**]$_0$: [**AIBN**]$_0$ = 0.5 M: 0.5 M: 0.05 M at 70 °C), we found the polymerization to reach high conversion (p = 0.993) after 4 hours as determined by ^{1}H-NMR analysis (**Figure S1**).

We evaluated the molecular weight of the reaction mixture throughout the polymerization by conventional SEC analysis in tetrahydrofuran (THF) using polystyrene standards (**Figure S2**).[19] To verify the polymerization mechanism, we decided to fit our experimental data to the original equations derived by Flory,[20] including theoretical number-average (M_n, eq 1), weight-average (M_w, eq 2), and Z-average (M_z, eq 3), that describes linear step-growth molecular weight evolution with respect to extent of reaction (p). Where M_o is the average molecular weight of the two reagents. It is important to note, that these theoretical molecular weight averages reflect the molecular weight distribution from crude reaction mixture and assumes no cyclization.[20]

COMMUNICATION

Table 1 Polymerization and characterization of $A_2 + B_2$ RAFT step-growth polymers with commercially available bismaleimide monomers.

Structure[a]	Time (h)[b]	p[c]	$r_{th,AIBN}$[d]	Reaction mixture		isolated					
				$M_{w,th}$[e]	$M_{w,PS}$[f]	$M_{w,LS}$[g]	$Đ_{LS}$[g]	$(M_z/M_w)_{LS}$	α[h]	T_g (°C)[i]	T_5 (°C)[j]
P(**M₂ₐ**-*alt*-**CTA₂**)	4	0.993	0.949	28k	25k	37.9k	1.70	1.67	0.571	79	232
$r = 0.980$	4	0.994	0.930	23k	20k	26.8k	1.62	1.59	0.597		
$r = 0.935$	4	0.996	0.889	15k	14k	19.0k	1.50	1.49	0.567		
$r = 0.818$	4	0.998	0.782	7.6k	8.0k	12.5k	1.35	1.36	0.531		
P(**M₂ᵦ**-*alt*-**CTA₂**)	21	0.942	0.891	9.3k	13.1k	15.4k	1.57	1.50	0.609	73	234
P(**M₂c**- *alt*-**CTA₂**)	2	0.995	0.970	57k	55.6k	69.0k	1.98	2.19	0.531	89	233
P(**M₂ᴅ**- *alt*-**CTA₂**)	4	0.967	0.949	14k	13k	20.9k	1.42	1.39	0.595	70	229

[a.] Polymerization conducted under stoichiometric conditions ($r = [M_2]_0/[CTA_2]_0$). [b.] Duration of the polymerization. [c.] monomer conversion determined by ¹H-NMR. [d.] Theoretical imbalanced stoichiometry from initiator assuming initiation efficiency of $f = 0.65$ using eq. 6. [e.] Theoretical weight average molecular weight taking into account the initiator derived imbalanced stoichiometry. [f.] Experimental M_w of the reaction mixture by conventional SEC analysis using polystyrene calibration. [g.] Molecular weight analysis by SEC with light scattering detector ($Đ = M_w/M_n$). [h.] Exponent parameter of Mark-Houwink plot. [i.] Glass transition temperature (T_g) measured by DSC analysis. [j.] Decomposition temperature at 5 % weight loss (T_5) measured by TGA analysis

$$M_{n,th} = M_0 \frac{1}{1-p} \quad (1)$$

$$M_{w,th} = M_0 \frac{1+p}{1-p} \quad (2)$$

$$M_{z,th} = M_0 \frac{1+4p+p^2}{1-p^2} \quad (3)$$

Pleasingly, we found the evolution of molecular weight averages by M_n, M_w, and M_z from SEC analysis to follow theoretical molecular weight averages from the equations above (**Figure 1A**). As seen in our original report,[7] the formation of oligomeric cyclic species significantly lowers the M_n and results in higher dispersity ($Đ = M_w/M_n$) (**Figure S2, Table S1**).

Next, we investigated the effect of imbalanced stoichiometry using excess **CTA₂** (**Figure 1B**, **Figure S4**). In theory, stoichiometric imbalance (r) between the chain end functionalities (i.e., $r = N_A/N_B$ in $A_2 + B_2$ step-growth) results in lower molecular weight at given conversion (p), which is commonly described for theoretical M_n (see eq 4). Imbalanced stoichiometry can also be considered for theoretical M_w and M_z by simply replacing p with $r^{1/2}p$ in eq 2 and 3.[20] Indeed, we found lower experimental molecular weight averages with increasing excess of **CTA₂** ($r = [M_2]_0/[CTA_2]_0 = 0.98, 0.93, 0.818$) which followed theoretical values predicted by eq 4 and modified equation 2 and 3 by replacing p with $r^{1/2}p$. (**Figure S5, Table S1**).

$$M_{n,th} = M_0 \frac{1+r}{1+r-2rp} \quad (4)$$

Given that AIBN was employed as a radical source in our polymerizations, imbalance in stoichiometry would be expected because of monomer loss from initiation (**Scheme S2**). Without considering the effect of radical termination, the overall

stoichiometric imbalance can be approximated by using equation 5:

$$r_{th,AIBN} = \frac{1}{\frac{1}{r} + 4f\frac{[I]_0}{[M]_0}(1-e^{-k_dt})} \quad (5)$$

Where k_d is the decomposition rate of the initiator and t is time. Here, 0.65 is assumed as a constant value for initiation efficiency (f) of the initiator radical specie.[21] Note an overall factor of 4 is in the denominator since each AIBN would create 2 radical species and assumes each initiator end group results in double the quantitative effect of the excess bifunctional reagent in molecular weight.[22] It is important to note, variation of overall initiation efficiency of the initiator (f) would result in significant difference in predicted molecular weight at high conversion. In addition, we want to emphasize that initiation efficiency of azo-initiators typically falls at high monomer conversion.[21] Nonetheless, replacing r with $r_{th,AIBN}$ (or replacing p with $r_{th,AIBN}^{1/2}p$ in eq 2) generally results in theoretical M_w closer to the experimental values (**Table 1**, **Table S1**).

Following the success of **M₂ₐ** as a RAFT step-growth comonomer with **CTA₂**, we next examined bis(3-ethyl-5-methyl-4-maleimidophenyl)methane (**M₂ᵦ**) (**Figure 1B**) and 2,2-bis[4-(4-maleimidophenoxy)phenyl]propane (**M₂c**) (**Figure 1C**) that are structurally analogous to **M₂ₐ**, using stoichiometrically balanced conditions above. During the polymerization of **M₂ᵦ**, we found the phenyl ring protons to shift towards the maleimide ring protons (**Figure S7**), which was not ideal to determine accurate conversion. Nonetheless, based on our approximation with the obtained NMR spectra, we found the polymerization to reach 83 % conversion after 4 hours, which was consistent with the molecular weight determined by SEC analysis (**Figure S8**, **Table S2**). In the literature, *N*-aromatic maleimides containing alkyl

ortho-substituents are reported with reduced radical polymerization rates,[23] which would account for the slower rate of polymerization of **M2B** when compared with **M2A**. Moderate molecular weight was achieved by leaving the polymerization for longer duration (**Table S2**); however, limited molecular weight would be expected if higher consumption of initiator from prolonged polymerization time leads to more significant imbalance in stoichiometry. In addition, it is noteworthy that there were noticeably less oligomeric cyclic species by SEC analysis (**Figure S8**), yielding $Đ$ values of the reaction mixture closer to the expected value of 2 for step-growth polymerizations (**Table S2**).[20] We speculate that the steric hindrance imparted by the alkyl-substituents on the maleimides would reduce the flexibility of the linear polymeric chain for the cyclization to occur.

On the other hand, **M2C**, which bears O-phenyl substituent *para* to the maleimide unit (**Figure 1C**), was observed to reach high conversion (p = 0.995, **Figure S10**) and high molecular weight (**Figure S11**) (M_w of 69 kDa by SEC via light scattering detector, corresponding to a weight-average DP of 120, or number-average DP of 60, **Figure S30**) after just 2 hours using the same reaction conditions, suggesting the O-phenyl substituent *para* to the maleimide unit increases the monomer reactivity. Leaving the reaction for 4 hours, on the other hand, resulted in noticeable high molecular weight shouldering, which was out of measurement range by our SEC analysis (**Figure S12**). It is important to note that M_z/M_w values were also higher than expected (**Table 1**, **Table S3**), suggesting some deviation from linear step-growth molecular weight evolution due to possible branching.

Lastly, we examined the RAFT step-growth polymerization with 4,4 substituted phenylene bismaleimide, **M2D**, which bears maleimide substituents attached on the same aromatic ring as **M2A** (**Figure 1D**) but having a more rigid structure. Due to the lack of solubility of **M2D**, we employed *m*-cresol as the solvent, though determining monomer conversion by ^{1}H-NMR was slightly cumbersome due to the maleimide C*H*=C*H* protons overlapping with peaks derived from the solvent (**Figure S14**). Furthermore, we anticipated the potential radical inhibiting effects of phenolic functionality in cresol could be detrimental to the polymerization.[24] Pleasingly, we found the polymerization of **M2D** and **CTA2** was able to reach high conversion within 4 hours (p = 0.967, **Table S4**). In addition, good agreement of molecular weight averages with expected values from conversion (**Figure 1D**, **Figure S15**) suggests minimal impact of the solvent. It is worth to mention that, in contrast to **M2B**, there were noticeable presence of cyclic specie in the RAFT step-growth polymerization of **M2D** (**Figure S15**); this is likely promoted by proximity and orientation of the maleimide units on **M2D**.

In all cases, we found that two or three rounds of precipitation was sufficient to remove most of the cyclic species without suffering from significant loss in yield (**Figures S3**, **S6**, **S7**, **S13**, **S16**). Importantly, we found the NMR spectrums of the isolated polymers to be consistent with the proposed structure (**Figures S17-S24**). To assess the conformation of the isolated polymers by Mark–Houwink–Sakurada (MHS) plots, we
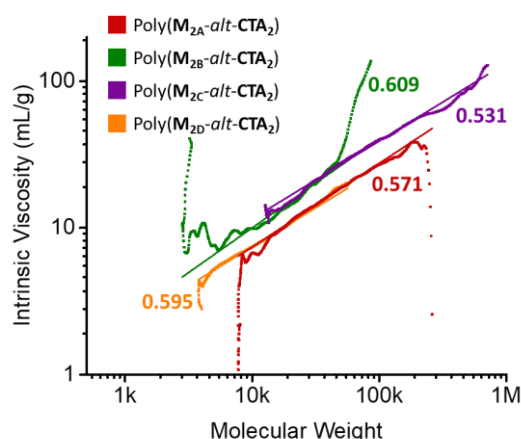

Figure 2. Mark-Houwink plot of the RAFT-step growth polymers in THF.

determined the intrinsic viscosity as a function of molecular weight by multi-detector SEC analysis (**Figure S25-S31**). The slope of this log-log plot corresponds to α that describes the evolution of intrinsic viscosity with molecular weight of the species as an exponent parameter (**Figure 2**).[25] In all cases studied here, the α value of the RAFT step-growth polymers was found to be between 0.55 to 0.6, which is consistent with structure-property relationship of linear polymers.[25] In contrast, branched polymers exhibit lower intrinsic viscosity relative to their molecular weight and yield α values less than 0.5 as they have more compact structures.[26]

We next examined the thermal stability of the RAFT step-growth polymers by thermal gravimetric analysis (TGA) (**Table 1**, **Figures S32-35**). Interestingly, all the linear backbone polymers showed moderate thermal stability with typical T_5 values above 220 °C and two step thermal degradation profiles. Furthermore, 30-45 % mass loss between 220 to 280 °C was observed, consistent with thermal cleavage of trithiocarbonate from the polymer backbone.[27, 28] It's noteworthy, Poly(M2c-alt-CTA2) displayed minor weight loss (3.5%) between 100 to 175 °C, which suggests the polymer to be the least stable. In addition, these polymers exhibited glass transition temperature (Tg) by Differential Scanning Calorimetry (DSC) analysis (**Table 1**, **Figure S36-39**), revealing the amorphous nature of the polymer backbone.

Finally, given the success in synthesis and affordability of the starting materials, we attempted to scale up the RAFT step-growth polymerization with **M2A**, and successfully isolated 8.1 grams of the P(**M2A**-*alt*-**CTA2**) (**Figure 3A**). To demonstrate the utility of RAFT step-growth backbone to prepare graft copolymers, we explored *N*-acrylomorpholine (NAM) to graft the side chains with (**Figure 3**). It is important to note that relatively small amount of the linear RAFT step-growth backbone by weight is sufficient to prepare graft copolymers as the sidechain monomers constitute majority of the molecular weight in the graft copolymers. For example, using 1.2 grams of P(**M2A**-*alt*-**CTA2**) we successfully prepared 15 grams of P(**M2A**-*alt*-**CTA2**-*g*-PNAM) (93 % recovery) (**Figure 3B**). Here, we used a monomer to CTA ratio of 40 ([NAM]$_0$/[CTA]$_0$ = 40) in dioxane ([NAM]$_0$ = 3M) and AIBN as the initiator at 65 °C ([CTA]$_0$/[AIBN]$_0$
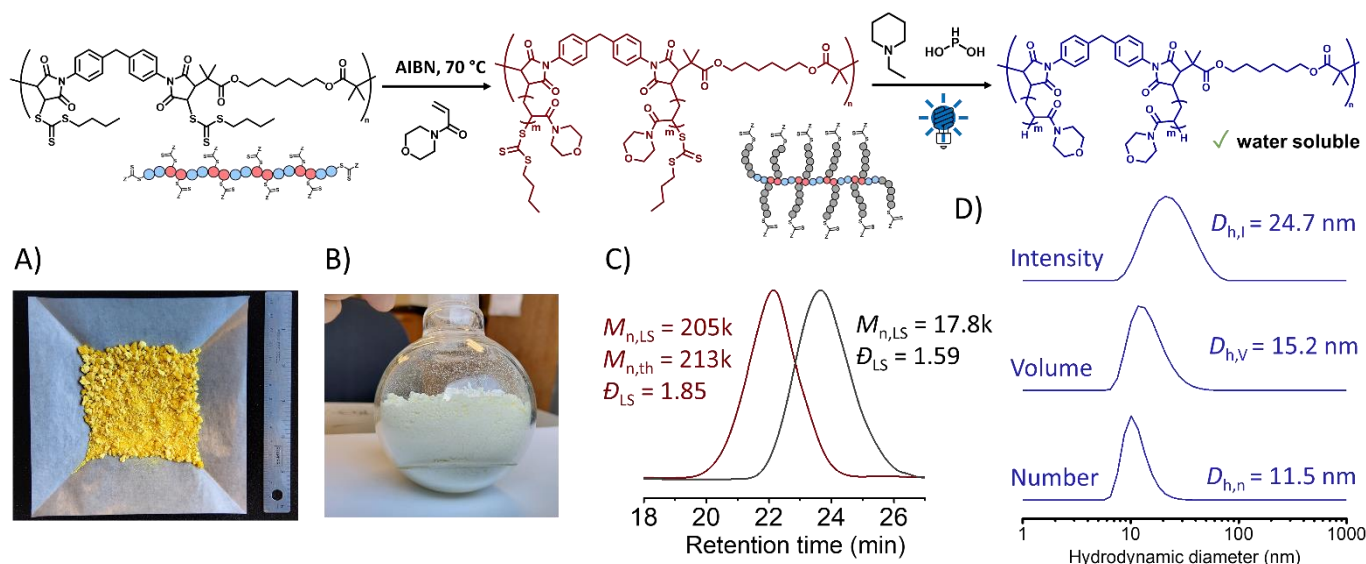
Figure 3. Large scale synthesis of graft copolymers from RAFT step-growth backbone and CTA end group removal. A) Photograph of 8.1 grams of P(M_{2A}-*alt*-CTA_2) (81 % yield).15 cm ruler is placed to represent the scale. B) Photograph of 15 grams of P(M_{2A}-*alt*-CTA_2-*g*-PNAM) (93 yield) in 250 ml round bottom flask. C) SEC-dRI traces of P(M_{2A}-*alt*-CTA_2) (black line) and P(M_{2A}-*alt*-CTA_2-*g*-PNAM) (red line). Molecular weights ($M_{n,LS}$ and $Đ_{LS}$) measured from the light scattering detector. $M_{n,th}$ is calculated from the ratio of NAM to CTA functionality and conversion of the NAM, multiplied by the number of grafting side chains based on the $M_{n,LS}$ of the precursor backbone. D) DLS traces (intensity, volume and number distribution) of the P(M_{2A}-*alt*-CTA_2-*g*-PNAM) in water (10 mg/ml) after end group removal.

= 40), which yielded $p \approx 99.6$ % after 2.5 hours (**Figure S40**). Successful synthesis of the graft copolymers was observed by apparent shift in SEC distribution and M_n by light scattering detector, which are consistent with the expected molecular weight of the graft copolymer from the M_n of the backbone measured (**Figure 3C**, **Figure S42**).

Graft copolymers have increasingly interested due to their unique rheological and mechanical properties,[29] applications are seen in lubrication[30] and tissue engineering.[31] Furthermore, as a single macromolecule of the size of colloids, they offer a modular platform for application in nanomedicine.[32]

Poly(*N*-acrylomorpholine) (PNAM) has attracted interest for biomedical applications as potential alternative to polyethylene glycol (PEG).[33] Although linear PNAM is typically reported to be water soluble,[34] we found our freshly prepared P(M_{2A}-*alt*-CTA_2-*g*-PNAM) to be insoluble in water. We attribute this peculiarity to the terminal end groups in brush topologies of our graft copolymers having a greater impact on solubility than end groups of linear polymers. Similarly, Reineke et al have shown the end groups to have significant effect on water solubility on brush polymers with *N*-alkyl acrylamide grafts.[35] Following CTA end group removal using light and *N*-ethyl piperidine hypophosphate (EPHP) (**Figure S41, S43**),[36] we found the resulting PNAM graft copolymer to be completely water soluble. Characterization of the resulting polymers via DLS (dynamic light scattering) displayed Z-average hydrodynamic diameter of 22 nm and overall polydispersity index (PdI) of 0.210 (**Figure 3D**), which we hypothesize to be single chain nanoparticle. To confirm this, DLS analysis was carried out in dimethylformamide (DMF) (**Figure S44**), where both the backbone and PNAM side chains are both freely soluble, revealing similar size distributions to aqueous condition. Indicating as a single macromolecule with desirable size for applications in tumour targeted drug delivery.[37, 38] It's important to emphasize, our modular nature of the step-growth backbone offers facile synthetic route for biological clearance.[7, 39]

In summary, we demonstrated RAFT step-growth polymerization using commercially available and cheap *N*-substituted bismaleimide monomers. In all cases (four examples), the evolution of molecular weight averages with conversion and intrinsic viscosity as function of molecular weight were both consistent with linear step-growth polymerization. We anticipate the use of the commercially available monomers will provide an easy access to these unique backbones, allowing chemist to focus on designing bifunctional CTA to provide functionality along a linear polymer or graft copolymers.

Author Contributions

The manuscript was written through contributions of all authors.

Conflicts of interest

The authors declare the following competing financial inter-est(s): J.T. and W.Y. are named inventors on the provisional patent application described in this work.

Acknowledgments

Notes and references

1. Y. Ikada and H. Tsuji, *Macromol. Rapid Commun.*, 2000, **21**, 117-132.
2. J. C. Worch and A. P. Dove, *ACS Macro Letters*, 2020, **9**, 1494-1506.
3. M. Riede, D. Spoltore and K. Leo, *Advanced Energy Materials*, 2021, **11**, 2002653.
4. A. Bossion, K. V. Heifferon, L. Meabe, N. Zivic, D. Taton, J. L. Hedrick, T. E. Long and H. Sardon, *Prog. Polym. Sci.*, 2019, **90**, 164-210.
5. J. Chiefari, Y. K. Chong, F. Ercole, J. Krstina, J. Jeffery, T. P. T. Le, R. T. A. Mayadunne, G. F. Meijs, C. L. Moad, G. Moad, E. Rizzardo and S. H. Thang, *Macromolecules*, 1998, **31**, 5559-5562.
6. N. Corrigan, K. Jung, G. Moad, C. J. Hawker, K. Matyjaszewski and C. Boyer, *Prog. Polym. Sci.*, 2020, **111**, 101311.
7. J. Tanaka, N. E. Archer, M. J. Grant and W. You, *J. Am. Chem. Soc.*, 2021, **143**, 15918-15923.
8. J. B. McLeary, F. M. Calitz, J. M. McKenzie, M. P. Tonge, R. D. Sanderson and B. Klumperman, *Macromolecules*, 2004, **37**, 2383-2394.
9. S. Houshyar, D. J. Keddie, G. Moad, R. J. Mulder, S. Saubern and J. Tsanaktsidis, *Polym. Chem,*, 2012, **3**, 1879-1889.
10. J. J. Haven, M. Hendrikx, T. Junkers, P. J. Leenaers, T. Tsompanoglou, C. Boyer, J. Xu, A. Postma and G. Moad, in *Reversible Deactivation Radical Polymerization: Mechanisms and Synthetic Methodologies*, American Chemical Society, 2018, vol. 1284, ch. 4, pp. 77-103.
11. D. J. Keddie, *Chem. Soc. Rev.*, 2014, **43**, 496-505.
12. B. Quiclet-Sire, G. Revol and S. Z. Zard, *Tetrahedron*, 2010, **66**, 6656-6666.
13. Z. Huang, B. B. Noble, N. Corrigan, Y. Chu, K. Satoh, D. S. Thomas, C. J. Hawker, G. Moad, M. Kamigaito, M. L. Coote, C. Boyer and J. Xu, *J. Am. Chem. Soc.*, 2018, **140**, 13392-13406.
14. J. Xu, C. Fu, S. Shanmugam, C. J. Hawker, G. Moad and C. Boyer, *Angew. Chem. Int. Ed.*, 2017, **56**, 8376-8383.
15. S. Lin, L. Zhang, Z. Huang, P. V. Kumar and J. Xu, *Macromolecules*, 2019, **52**, 7157-7166.
16. Y. Zhou, Z. Zhang, C. M. Reese, D. L. Patton, J. Xu, C. Boyer, A. Postma and G. Moad, *Macromol. Rapid Commun.*, 2020, **41**, 1900478.
17. R. Liu, L. Zhang, Z. Huang and J. Xu, *Polym. Chem,*, 2020, **11**, 4557-4567.
18. Z. Li, J. Li, X. Pan, Z. Zhang and J. Zhu, *ACS Macro Letters*, 2022, DOI: 10.1021/acsmacrolett.1c00762, 230-235.
19. M. Gavrilov and M. J. Monteiro, *Eur. Polym. J.*, 2015, **65**, 191-196.
20. P. J. Flory, *J. Am. Chem. Soc.*, 1936, **58**, 1877–1885.
21. G. Moad, *Prog. Polym. Sci.*, 2019, **88**, 130-188.
22. P. J. Flory, *Principles of polymer chemistry*, Cornell University Press, Ithaca, NY, 1953.
23. A. Matsumoto, T. Kubota and T. Otsu, *Macromolecules*, 1990, **23**, 4508-4513.
24. S. Fujisawa and Y. Kadoma, *Dent. Mater.*, 1992, **8**, 324-326.
25. Y. Lu, L. An and Z.-G. Wang, *Macromolecules*, 2013, **46**, 5731-5740.
26. A. B. Cook, R. Barbey, J. A. Burns and S. Perrier, *Macromolecules*, 2016, **49**, 1296-1304.
27. T. M. Legge, A. T. Slark and S. Perrier, *J. Polym. Sci., Part A: Polym. Chem.*, 2006, **44**, 6980-6987.
28. A. Postma, T. P. Davis, G. Moad and M. S. O'Shea, *Macromolecules*, 2005, **38**, 5371-5374.
29. M. Abbasi, L. Faust and M. Wilhelm, *Adv. Mater.*, 2019, **31**, 1806484.
30. X. Banquy, J. Burdyńska, D. W. Lee, K. Matyjaszewski and J. Israelachvili, *J. Am. Chem. Soc.*, 2014, **136**, 6199-6202.
31. M. Vatankhah-Varnosfaderani, W. F. M. Daniel, M. H. Everhart, A. A. Pandya, H. Liang, K. Matyjaszewski, A. V. Dobrynin and S. S. Sheiko, *Nature*, 2017, **549**, 497-501.
32. M. Müllner, *Macromol. Chem. Phys.*, 2016, **217**, 2209-2222.
33. K. M. Torres-Obreque, G. P. Meneguetti, J. J. Muso-Cachumba, V. A. Feitosa, J. H. P. M. Santos, S. P. M. Ventura and C. O. Rangel-Yagui, *Drug Discovery Today*, 2022, **27**, 65-81.
34. G. Gody, T. Maschmeyer, P. B. Zetterlund and S. Perrier, *Nature Communications*, 2013, **4**, 2505.
35. M. L. Ohnsorg, P. C. Prendergast, L. L. Robinson, M. R. Bockman, F. S. Bates and T. M. Reineke, *ACS Macro Letters*, 2021, **10**, 375-381.
36. R. N. Carmean, C. A. Figg, G. M. Scheutz, T. Kubo and B. S. Sumerlin, *ACS Macro Letters*, 2017, **6**, 185-189.
37. H. Cabral, Y. Matsumoto, K. Mizuno, Q. Chen, M. Murakami, M. Kimura, Y. Terada, M. R. Kano, K. Miyazono, M. Uesaka, N. Nishiyama and K. Kataoka, *Nature Nanotechnology*, 2011, **6**, 815.
38. S. Kaga, N. P. Truong, L. Esser, D. Senyschyn, A. Sanyal, R. Sanyal, J. F. Quinn, T. P. Davis, L. M. Kaminskas and M. R. Whittaker, *Biomacromolecules*, 2017, **18**, 3963-3970.
39. P. Shieh, H. V. T. Nguyen and J. A. Johnson, *Nature Chemistry*, 2019, **11**, 1124-1132.